Title

Daylight-activated fumigant detoxifying nanofibrous membrane based on thiol-ene click chemistry

Authors

Tang, Peixin
Sun, Gang

Publication Date

2021-03-01

DOI

10.1016/j.jhazmat.2020.124723

Peer reviewed

HHS Public Access

Author manuscript

J Hazard Mater. Author manuscript; available in PMC 2022 March 15.

Published in final edited form as:

J Hazard Mater. 2021 March 15; 406: 124723. doi:10.1016/j.jhazmat.2020.124723.

Daylight-activated fumigant detoxifying nanofibrous membrane based on thiol-ene click chemistry

Peixin Tang, **Gang Sun***

Department of Biological and Agricultural Engineering, University of California, Davis, CA, 95616, USA

Abstract

Daylight-activated detoxifying nanofibrous membranes (LDNMs) are fabricated by grafting benzophenone-3,3',4,4'-tetracarboxylic dianhydride (BD) and biological thiols successively on poly(vinyl alcohol-co-ethylene) (EVOH) nanofibrous membrane. Taking the merits of photoactivity of BD, high-reactivity of biological thiols, and high specific surface area and porosity of the nanofibrous membrane, 1,3-dichloropropene (1,3-D) can be efficiently detoxified on the LDNMs under daylight irradiation via a thiol-ene click reaction. The detoxification function of the LDNMs is "switched on" by light irradiation and continues by following a cascade of chemical attacks of thiyl radicals formed during the photoexcitation process. The resultant LDNMs present rapid detoxification rate (i.e., $t_{1/2}$ = ~30 min) and massive detoxification amount (i.e., ~12 mg/g) against 1,3-D vapor under ambient conditions. More importantly, the LDNMs perform a detoxification tailing effect after moving the light-irradiated membrane to a dark environment, thus ensuring the protective function in the absence of sufficient light sources. The detoxification property of the LDNMs in an outdoor environment with sunlight irradiation shows comparable results to the lab-scale outcomes, enabling them to serve as innovative materials for personal protective equipment in practical applications. The successful fabrication of LDNMs may inspire new insights into the design of protective materials providing aggressive protection.

Keywords

photochemistry; 1,3-dichloropropene; protective material; thiol-ene click reaction; detoxification

1. Introduction

The wide application of pesticides is necessary to maintain sufficient agricultural production of food crops. However, the accumulation, distribution, and resettlement of pesticide residues pose health threats to human beings and the environment, since most pesticides are either highly toxic or long-term persistent in the environment for months to years [1–5]. Fumigants are a group of highly volatile chemicals that are commonly used as pre-plant pesticides to control the growth of soil-born pests, mostly for strawberry productions in California, USA [6]. Given the ban of methyl iodide and methyl bromide, 1,3-dichloropropene (1,3-D) has been considerably used as an alternative in agricultural

*Corresponding author: Tel.: +1 530 752 0840; gysun@ucdavis.edu (G. Sun).

production [7]. According to a report from the California Department of Pesticide Regulation (Cal DPR), the annual usage of 1,3-D was 12.5 million pounds in 2017, ranked at No. 3 over one hundred pesticides [8]. On the other hand, the acute and chronic toxicity of 1,3-D drove the regulation of its permissible exposure limit at 1 ppm for an average exposure duration of 8 hours [9]. The overexposure of 1,3-D can cause respiratory, eye, and skin irritation, and 1,3-D is listed as a probable carcinogen to human beings [7,9]. Therefore, the development of novel personal protective equipment (PPE) against 1,3-D exposure is urgent and necessary for occupational and personal safety.

Due to the high specific surface area, high porosity, and light weight of nanofibrous membranes, they have been extensively designed as novel functional materials to provide passive or aggressive protection against biological [10,11] and chemical [12] hazards. The newly emerged defensive materials against organophosphorus pesticides, also known as chemical warfare agents, mostly follow passive adsorption mechanism relying on highly porous activated carbon [13,14]; provide aggressive protection based on catalytic hydrolyses or redox reactions [15–21]; or perform detoxification based on enzyme-assisted systems [22,23]. On the contrary, the developments of PPE against fumigant exposures are very limited in reports but crucial for the safety of farmworkers and residents who live nearby the fields. Due to the fact that fumigants are highly volatile, colorless, and odorless, exposure to the fumigant is usually unnoticeable yet can lead to severe adverse outcomes. Nanofibrous-based colorimetric sensors for detecting fumigants were designed to show naked-eye readable signals toward ppb-ppm levels of fumigants, providing the first layer of protection against overexposure [24–27]. However, the lack of strategies to detoxify fumigants in the environment still poses potential health risks to human beings, especially to children. The decontamination of 1,3-D in water and soil by polysulfides and ammonium thiosulfate was studied, and the mechanism was investigated as a dehalogenation process of 1,3-D. However, the chemicals took 5–25 hours to decontaminate 0.5 mM of 1,3-D because of the relatively inert C-Cl bond in the 1,3-D structure [28,29]. A hierarchical nucleophilic nanofibrous membrane was reported to present much faster 1,3-D detoxification, whereas the use of petroleum-based polymer highly limited its broad applications in terms of sustainability and environmental friendliness [12].

Light is a green, sustainable, and easily accessible energy, which can “switch on” versatile functions on fibrous materials including anti-microorganisms [10,30], photocatalysis [16], and chemical decontamination [16,31,32]. Specifically, Yan L., et al., designed a composite based on $CuInS_2$/ZnS:Al-sensitized TiO_2 to detoxify 1,3-D through photodegradation. With the optimized composite, 92% of 1,3-D can be degraded within 5 hours of UV irradiation [32]. Thiol-ene click reaction, which can be triggered with the presence of photoinitiator/photosensitizers and light, is popularly used in polymeric material syntheses due to its fast rate, high yield, and good stereoselectivity [33,34]. However, based on our knowledge, the use of thiol-ene click reaction in capturing and rapid detoxifying fumigants under light irradiation has not been reported yet.

Herein, we introduce an approach of fabricating light-activated detoxifying nanofibrous membranes (LDNMs) against 1,3-D via thiol-ene click chemistry. Poly(vinyl alcohol-co-ethylene) (EVOH) nanofibrous membrane was used as a template to provide a high specific

surface area, benefiting the surface modification as well as the detoxification. The LDNMs were achieved by incorporating daylight-active benzophenone-3,3',4,4'-tetracarboxylic dianhydride (BD) and different thiols, mostly biological thiols, on the EVOH nanofibrous membrane through surface modifications. Here, BD not only works as a linker for the thiol modification but also plays an essential role as a photosensitizer on the LDNMs. Under daylight irradiation, LDNMs can be excited to trigger the formation of thiyl radicals, thereby "switching on" the detoxification reaction toward toxicants containing carbon-carbon double bond (i.e., ene-based toxicants). The light-activated detoxifying property of the as-designed LDNMs were characterized experimentally and theoretically. As a consequence, the LDNMs exhibit integrated properties of rapid detoxification, protection tailing effect, and long-term stability.

2. Experimental

2.1. Chemicals and materials

Poly(vinyl alcohol-co-ethylene) (ethylene content = 27%) (EVOH), benzophenone-3,3',4,4'-tetracarboxylic dianhydride (BD), L-cysteine hydrochloride anhydrous (CYS), hexane, tetrahydrofuran (THF), isopropanol (IPA), and polyphosphoric acid (PPA) were purchased from Sigma-Aldrich (St. Louis, MO, USA). Cysteamine hydrochloride (CA), 1,3-dichloropropene (isomer mixture) (1,3-D), and N, N'-dimethyl-4-nitrosoaniline (*p*-NDA) were purchased from Spectrum Chemicals & Laboratory Products (Gardena, CA, USA). 1-Ethyl-3-(3-dimethylaminopropyl)carbodiimide hydrochloride (EDC) was bought from the Advanced ChemTech (Louisville, KY, USA). Ellman's reagent (5,5'-dithiobis-(2-nitrobenzoic acid)) was bought from Thermo Scientific (Waltham, MA, USA). Reduced $_{L}$-glutathione (GSH) and ethane-1,2-dithiol (diSH) were purchased from TCI (Portland, OR, USA). All chemicals were directly used as received.

2.2. Preparation of EVOH nanofibrous membrane

EVOH (8 wt%) was dissolved in a solvent of H_2O/IPA= 3/7 (v/v) by vigorously stirring at 80 °C for overnight. Then, the viscous polymer solution was pumped into plastic syringes with metallic needles, and the electrospinning was performed under a high voltage of 23 kV. The pumping rate of the polymer solution was controlled at 1 mL/h. The EVOH nanofibrous membranes were collected in a metallic roller covered with wax paper and connected to the ground. Finally, the resultant nanofibrous membrane was peeled out from wax paper (purchased from Reynolds, IL, USA) and stored for further modifications.

2.3 Fabrication of LDNMs

Two steps were adopted to achieve the LDNMs. Firstly, the EVOH nanofibrous membrane was modified by BD to gain photoactivity according to previous work [10]. Specifically, the EVOH membranes (around 200 mg) were immersed in 50 mL of THF containing 5 wt% of BD with 1 wt% of PPA for 5 min. The solution was heated to 80 °C to fully dissolve BD and then cooled to room temperature before immersing the EVOH membrane. The EVOH membrane containing BD was completely dried under ambient conditions. Then, the dried membrane was cured at 120 °C for 30 min to perform an esterification reaction between EVOH and BD. Afterward, the BD-EVOH membrane was obtained by washing it with hot

THF and subsequent drying under a dark and ambient condition. Secondly, to incorporate sulfhydryl (–SH) groups onto the membranes, EDC was applied as an activating agent to facilitate the coupling reaction between the carboxyl on the BD-EVOH and the amine group in thiols. Here, biological thiols (including L-glutathione, L-cysteine, and cysteamine) and ethane-1,2-dithiol were selected for fabrications of LDNMs. Specifically, BD-EVOH (20 mg) was immersed in 1.0 wt% of EDC/phosphate-buffered saline (PBS) solution (10 mL, pH=7.4) at room temperature for 30 min for activation of carboxylic groups. Then, the activated BD-EVOH was transferred into 10 mL of PBS solution containing 0.5 mmol of thiols. The solution mixture was purged with N_2 gas to minimize the oxidation of –SH groups during the modification. Then, the modification was performed under room temperature for 90 min with a magnetic stirrer. The resultant LDNMs were obtained by washing the membrane with water, acetone, and hexane, and dried under dark and ambient conditions. No bad smells were found in the resultant membranes except for the one incorporated with diSH (BDdiSH-LDNM).

2.4. LDNMs characterization

Attenuated total reflectance-Fourier transform infrared (ATR-FTIR) spectroscopy (Nicolet 6700 FTIR spectrometer, Thermo Electron Co., MA, USA) was employed to analyze the structural changes of the membrane during the preparation processes. The absorbance of the spectrum was acquired in the range of 400–4000 cm^{-1} with a resolution of 2 cm^{-1}. Scanning electron microscope (SEM) images were captured by a field emission-SEM (FE-SEM) of Quattro ESEM (Thermo Fisher Scientific, MA, USA). The quantification of –SH groups on the membrane was achieved by using Ellman's reagent [35]. Specifically, precisely weighted 2 mg of LDNM was immersed in 2.5 mL of PBS buffer, then 50 μL of 10 mg/mL Ellman's reagent was added into the solution. The mixture was incubated at room temperature for 10 min, then the color intensity of the solution was scanned in a UV-vis spectrophotometer (Evolution 600, Thermo Fischer). The absorbance at 412 nm (A_{412}) was recorded and converted to the –SH concentration in a unit of mM in solution (C_{SH}) according to a self-established calibration curve ($A_{412} = 1.6959C_{SH} + 0.0576$, $R^2 = 0.9996$). ^1H Nuclear Magnetic Resonance (NMR) was performed on a Brucker 400 MHz NMR (Bruker Co., MA, USA) by using DMSO-d_6 as a solvent.

2.5. Measurement of ROS production

LDNMs (2 cm ×2 cm) were immersed in 10 mL of 40 μM *p*-NDA solution in a glass petri dish. Here, *p*-NDA was selected as a highly selective hydroxyl radical scavenger which shows a color fading after reacting with hydroxyl radicals [36]. The samples were exposed to daylight or UVA in an XL-1500 crosslinker for different durations. The light intensity in the crosslinker was measured by two types of light meters as 13 kLux (EXTECH, Model # LT300) and 80 μW/cm^2 (Fisher Scientific, Ultra-Violet Radiometer) for daylight and UVA, respectively. The color fading of the *p*-NDA solution was detected with a UV-vis spectrophotometer, and the *p*-NDA concentrations ($C_{p\text{-NDA}}$) in a unit of 1×10^{-5} M before and after light irradiation were calculated according to a calibration curve ($A_{440} = 0.3387\times C_{p\text{-NDA}} - 0.0095$, $R^2 = 0.9998$) measured at the absorbance intensities of standard *p*-NDA solutions at the maximum absorption wavelength of 440 nm (A_{440}).

2.6. Detoxification function of LDNMs

LDNM (~8 mg) was incubated with specific concentrations of 1,3-D in the gas phase in a 5 mL glass vial with different durations of light irradiation (daylight or UVA). The 1,3-D solutions were prepared in hexane since it was tested to be inert to –SH groups on the LDNMs during light irradiation. The residual concentration of fumigant vapor in the vial was quantified through a colorimetric method by using *p*-(4-nitrobenzyl) pyridine (NBP) as the colorimetric probe. In detail, 30 wt% of NBP was dissolved in acetone, 1 mL of the NBP solution was injected into the vials after the detoxification. Then, the vial was incubated in an oil-bath at 70 °C for 10 min. The color change of the NBP solution after incubation was measured by the UV-vis spectrophotometer, and the residual concentration of 1,3-D in the unit of μg/mL NBP/acetone solution ($C_{1,3\text{-}D}$) was calculated according to a calibration curve based on the absorption intensity at λ_{max} = 547 nm (A_{547}): $A_{547} = 0.007C_{1,3\text{-}D} + 0.1032$, $R^2 = 0.9975$.

2.7. Gaussian calculations

All theoretical calculations were performed using Gaussian 09. The optimized geometries at the ground state were obtained at density functional theory (DFT)-B3LYP/6–31+G(d,p) level of theory in the gas phase. The excitation phenomenon of the compounds was calculated using time-dependent density functional theory (TD-DFT)-B3LYP/6–31+G(d,p) level of theory in the gas phase. The Gibbs free energy of the compounds with their ground state or excited state geometries were obtained through the frequency calculation. The calculation results were visualized with GaussView 5.0.8.

3. Results and discussion

3.1. Fabrication of light-activated detoxifying nanofibrous membranes (LDNMs)

The LDNMs against overexposure of ene-based toxicants were designed to fulfill three required performances: (1) the membranes can efficiently adsorb and interact with toxicants, (2) the membranes must show effective detoxification function under light irradiation, and (3) the detoxification function of LDNMs must be unique to ene-based toxicants with negligible environmental interferences. Taking the merit of ultrahigh specific surface area and high porosity of the nanofibrous membrane, it was applied as the template to fulfill the first criterion with efficient adsorption and rapid reaction against toxicants as well as good air permeability. To satisfy the latter two requirements, radical-mediated thiol-ene chemistry was chosen as the detoxification reaction to provide chemical protection against ene-based toxicants under light exposure. Specifically, the molecular design of the LDNMs was achieved by covalently bonding benzophenone structure with biological thiols on surfaces of the nanofibrous membranes. The benzophenone group has high photoactivity and is widely used as a photosensitizer to initiate free radical polymerization. In this case, the LDNMs integrated the photosensitizer and sulfhydryl groups on the membranes, thus performing detoxification function via photo-induced thiol-ene click reaction. Fig. 1a presents four synthesized structures of LDNMs. EVOH was used as the template to construct the nanofibrous networks via electrospinning, whose average fiber diameter was around 400 nm (Fig. S1). The massive hydroxyl groups in EVOH allow its covalent functionalization by BD (i.e., the photosensitizer) through an esterification reaction. Thereafter, the –SH groups were

further endowed by linking biological or synthetic thiol compounds on the membrane based on coupling reactions between the carboxyl in BD-EVOH and the amino/thiol groups in thiol compounds under EDC activation (Scheme S1). Here, three biological thiols (i.e., CYS, GSH, and CA) and one synthetic thiol (i.e., diSH) were applied as the sulfhydryl sources to the designed LDNMs. The resultant membranes were denoted as BDCYS, BDGSH, BDCA, and BDdiSH when CYS, GSH, CA, and diSH were respectively used. Under SEM monitoring, the LDNMs presented randomly distributed nanofibers, showing flat and molten morphology, with an average fiber diameter of around 800 nm (Fig. 1b). This change mostly happened during the BD modification since organic acid, high temperature, and long-term curing were adopted, resulting in nanofiber swelling, slight melting, and even potential crosslinking [37]. Eventually, the average fiber diameter of BD-EVOH has been doubled, but the membranes maintained their 3D net structures (Fig. S1). The average fiber diameters changed from 400 nm to 800 nm, slightly affected the specific surface area of the membranes [38]. Then, the fabrication of LDNMs was mildly achieved in an aqueous system at a neutral pH. No further fiber morphological changes were noticed, thus ensuring the ultrahigh specific surface area and massive porosity in the LDNMs, which are crucial for their detoxification efficiency. The importance of the nanofibrous structure of the material was demonstrated by comparing the detoxification efficiency between BDCA-LDNM and a non-porous BDCA-EVOH film (see fabrication method in Supplementary Material). As a result, the detoxification amount of 1,3-D by BDCA-EVOH film was tested as 5.36 mg/g, which was 2.3 times lower than that of the BDCA-LDNM after 30 min of daylight irradiation.

ATR-FTIR spectra were obtained to structurally characterize the membranes after different treatments (Fig. 1c). Compared with the EVOH, the covalent linkage of BD on the membrane was proved by the appearance of new peaks referring to the carboxyl and ester groups (1688–1712 cm^{-1}) and the anhydride groups (1780 cm^{-1} and 1845 cm^{-1}) in the BD-EVOH spectrum. After reacting with thiols, the anhydride peaks on the membrane decreased in different degrees and even disappeared in the spectra of BDCA-LDNM and BDdiSH-LDNM. Moreover, the emergence of a peak at 1601 cm^{-1} refers to amide or thioate groups (i.e., C=O stretching) linked between BD and thiols on the LDNMs. The presence of the benzyl substitution in BD moiety shifted the absorbance to the lower wavenumbers. The concentration of active –SH groups on the LDNMs was quantified by using Ellman's reagent [35]. The presence of free –SH groups on the LDNMs can break the disulfide bonds in the Ellman's reagent and produce a yellow ion (λ_{max} = 412 nm) in an aqueous solution, whose concentration can be quantified by the UV-vis spectrophotometer. As shown in Fig. 1d, the –SH concentration on the LDNMs containing different thiols varied greatly. The best performance was achieved on the BDCA-LDNM, whose –SH concentration (172.9 μmol/g) was 10–30 times higher than that of the ones modified by CYS, GSH, or diSH. The application of EDC-catalyzed coupling reaction for LDNM modification can ensure the efficient binding of CA to the BD moiety by forming amide bonds instead of the thioate [39]. This was also proved by a 28.7-folds higher of the –SH concentration on the BDCA-LDNM than that of the BDdiSH-LDNM (Fig. 1d). However, the presence of anionic carboxylic groups in CYS and GSH led to charge repulsions to the BD-EVOH membrane surfaces, resulting in lower thiol loadings on the resultant LDNMs. On the other hand, diSH

is reactive not only to the carboxyl group but also to ketones to form 1,3-dithiolanes, which is a common intermediate in organic synthesis [40]. The competitive reaction of diSH led to less targeted structure achievements on the LDNM (i.e., less free –SH groups) and could also affect the photoactivity of the LDNMs by consuming the carbonyl groups in the BD moiety (Scheme S1e).

Benzophenones are a group of typical photoactive compounds and commonly used as photosensitizers for radical-mediated polymerizations with UV or daylight irradiation [41,42]. Its high efficiency at the intersystem crossing (ISC) from its singlet excited state to the triplet state allows the production of biocidal reactive oxygen species (ROS) with the presence of light, hydrogen donor, and oxygen [10]. As shown in Fig. 1e, under light irradiation, the BD moiety in LDNM can be excited from its ground state (S_0) to multiple singlet state (S_n), and rapidly goes back to the lowest singlet excited states (S_1) through the internal conversion process. Then, the excited BD moiety can undergo the ISC to their triplet excited states, which is contributed as a bi-radical (see detailed mechanisms in Scheme S2). The achievement of the triplet excited state of BD moiety can effectively trigger thiyl radical formation on the LDNMs, “turning on” the thiol-ene click detoxification reaction. Herein, the light is a “switch” to control the detoxification function of the LDNMs. The proposed mechanisms of the photo-initiation and photo-activated detoxification against ene-based toxicants are illustrated in Fig. 1f [43]. The light irradiation hinges on the photoreaction of the ground state of LDNMs (LDNM-SH) accessed to its triplet excited state (^{3}LDNM-SH*) via the ISC process. Thereafter, ^{3}LDNM-SH* can abstract hydrogen from hydrogen donors in the surrounding environment to form benzophenone ketyl radical (LDNMH•-SH). In the case of LDNMs, the –SH groups on the membrane would be the favorable hydrogen donor, resulting in the generation of thiyl radical (LDNM-S•) and then “switching on” the detoxification cycle. The LDNM-S• can favorably target the ene groups in toxicants via anti-Markovnikov addition reaction to showcase the detoxification function of the LDNMs. After that, the detoxification will continuously perform by having freshly formed LDNM-S• via hydrogen abstraction either by ^{3}LDNM-SH* (step i) or the carbon-centered radicals formed during the detoxification process (step ii) (Fig. 1f).

Fig. 1g depicts the light-activated detoxification function of LDNMs against 1,3-D. Under light irradiation, it is expected to detoxify 1,3-D via thiol-ene click reaction by having readily formed thiyl radicals on the LDNM surfaces, performing protective functions. The LDNMs could be the candidates for the design of novel personal protective equipment with aggressive protection.

3.2. Photoactivity of LDNMs

Although the photoactivity BD-EVOH membrane has been thoroughly investigated previously [10], the nature of the photoexcitation process of LDNMs is the key to the protective function. To provide an insight on the photoactivity of LDNMs, which is essential to “switching on” the detoxification function of the LDNMs, we applied TD-DFT simulations and diffuse reflectance UV-visible (UV-vis) spectroscopy to investigate the photoexcitation process of different LDNMs. The maximum absorption wavelengths (λ_{max}) of BDCYS, BDGSH, BDCA, and BDdiSH were calculated as 297 nm, 289 nm, 303 nm, and

299 nm, respectively (detailed information is available in Table S1). The calculated λ_{max} of relevant LDNMs were highly consistent with the experimental results (Fig. 2a-d), proving the accuracy of the theoretical calculations. Also, the diffuse reflectance UV-vis spectra of EVOH and BD-EVOH are available in Fig. S1 for reference. By examining the frontier orbitals of the triplet excited state (T_1) of the LDNMs, all four LDNMs present n_{HOMO-n}-π^*_{LUMO} transition from the carbonyl group to the phenyl ring of the BD moieties (Fig. 2a-d), satisfying El-Sayed's rules to ensure the efficiency of ISC and to achieve their T_1 states [44,45]. Although the strongest absorptions of LDNMs are located in the UV range, the light energy of D65 lamps ranging from 300 to 400 nm can still be utilized in the photoexcitation of LDNMs (Fig. 2e).

To get an insight on the ability to form thiyl radicals with the photo-initiation of the LDNMs, which is a hydrogen abstraction process from the –SH group by the excited LDNMs (T_1), the electrostatic potential of the LDNMs were mapped and showed in Fig. 2f. Compared with the S_0 state of the LDNMs, their T_1 states showcased reduced electron deficiency on the oxygen atom of the carbonyl group in the BD moieties. It demonstrated the favorability of LDNMs in hydrogen abstraction and the feasibility of thiyl radical formation on the LDNMs. The formation of thiyl radicals mediated from the T_1 state of LDNMs (^{3}LDNM-SH*) was further predicted by calculating the Gibbs free energy changes (ΔG) of relevant LDNMs. As shown in Fig. 2g, the reactions between ^{3}LDNM-SH* and the S_0 state of LDNM (LDNM-SH) to produce LDNM-S• and LDNMH•-SH radicals in the gas phase are highly spontaneous by showing negative values of calculated ΔG (varying from –71.95 to –85.33 kJ/mol). Then, the generated LDNMH•-SH can be quenched by oxygen and produce ROS, like hydroxyl radical (HO•), which can be used as a marker to examine the occurrence of the photo-initiation cycle that was proposed in Fig. 1f. Experimentally speaking, the productions of HO• on the LDNMs under UVA or daylight irradiation were quantified by a colorimetric quencher of *p*-NDA, which indirectly illustrates the occurrence of the photo-initiation cycle. As shown in Fig. 2h, the HO• production efficiency is greatly different among the four LDNMs. BDCA showed the highest production of HO• with prolonged UVA exposure times. However, the efficiencies for BDCYS, BDGSH, and BDdiSH were much lower than that of the BDCA. For the BDCYS and BDGSH, the lower efficiency of HO• production can be attributed to the low thiol loading on the membrane, which was limited by lacking good H-donors (e.g., –SH groups) to promote the HO• production. On the other hand, although the loading capacity of diSH on the membrane was about three times higher than that of CYS and GSH, no obvious improvement was found on the HO• production, which further confirmed the interfered reaction between diSH and the carbonyl in BD moiety, thus destroying its photoactivity. Similarly, D65 can also trigger the photo-initiation of the LDNMs with slightly lower efficiency, demonstrating the robust utilization of daylight source to "switch on" the detoxification function of the LDNMs (Fig. 2i).

3.3. Light-activated detoxification function of LDNMs

The LDNMs were challenged by 1,3-D under UVA or daylight irradiation to evaluate their detoxification functions. As shown in Fig. 3a and 3b, BDCA-LDNM performed the best detoxification property against 1,3-D. The detoxification amount of 1,3-D gradually

increased to 12.02 mg/g and 9.59 mg/g by prolonging the UVA and D65 irradiation to 45 min, respectively. In these two cases, 76.58% and 61.17% of 30 μg/mL of 1,3-D were detoxified by the BDCA-LDNM under UVA and daylight, respectively. Here, the 1,3-D concentration refers to the amount of 1,3-D to the volume of the air in the glass vial. However, the detoxification of 1,3-D on the other three LDNMs were very limited, whose functions could be inhibited due to the low –SH group concentration or less efficient photo-initiation on the LDNMs. Thus, the BDCA-LDNM was applied to further examine its protective performance.

BDCA-LDNMs were exposed to different initial concentrations of 1,3-D under D65 lamps irradiation. As presented in Fig. 3c, the detoxification reached equilibrium within 30 min under all tested concentrations. The detoxification amounts on the BD-LDNM after 45-min of light irradiation were calculated as 12.16, 9.35, and 3.85 mg/g when the initial concentrations of 1,3-D were at 50, 30, and 10 μg/mL, respectively. The detoxification process was evaluated by fitting the process to the pseudo-first order kinetics (Fig. 3d), and the rate constants were calculated as –0.0303, –0.0326, –0.0205 min^{-1} with increasing the initial concentrations of 1,3-D from 10 to 50 μg/mL, respectively. After 45 min of daylight exposure, the residual –SH concentrations on the BDCA-LDNMs were quantified by Ellman's reagent. As shown in Fig. 3e, the –SH groups on the membrane were consumed in different degrees. More interestingly, the consumption amounts of the –SH groups were consistent with the detoxification amounts of 1,3-D stoichiometrically. By calculating the molar ratio of the consumed –SH groups to the detoxified 1,3-D (Δ–SH/Δ1,3-D), we found that the ratio swung around 1.0, which are 0.76, 1.03, and 1.03 when the 1,3-D initial concentrations were 10, 30, and 50 μg/mL, respectively. It further confirmed that the thiol-ene click reaction was dominated in the inactivation of 1,3-D with negligible interfered reactions, i.e., one mole of –SH reacted with one mole of 1,3-D. However, a small portion of the –SH groups was inactivated via side reactions (e.g., ROS oxidation) when the 1,3-D concentration was relatively low (e.g., 10 μg/mL) [46]. The detoxification capacity of the BDCA-LDNM was obtained as 12.39 mg/g by prolonging the daylight irradiation time to 90 min, which ensured the achievement of the detoxification equilibrium, with a 1,3-D initial concentration of 50 μg/mL. The complete consumption of –SH groups on the BDCA-LDNM was inhibited by the insufficient contact of the membrane to the 1,3-D vapor. It is worth to note that only 8.44% of –SH groups on the BDCA-LDNM was consumed solely by the side reactions induced by daylight irradiation (30 min), ensuring the robustness of LDNMs for practical application.

A detoxification tailing effect of the LDNMs ensures sufficient protection when losing the strong light irradiation. According to previous research [10], benzophenones can be partially converted to corresponding light-absorbing transient (LAT) structures after light irradiation, which can readily generate radical-mediated ROS with the presence of oxygen and good hydrogen donors under a dark condition. Then, the LAT structure will reform the benzophenone via a hydrogen abstraction process (Fig. 3f). Thus, BDCA-LDNMs were irradiated by daylight with increasing time durations, the formation of the LAT structure on the membrane was monitored by diffuse reflectance UV-vis spectroscopy (Fig. 3g). According to the TD-DFT calculation results, the LAT of BDCA shows the maximum absorbance at the wavelength of 406 nm (Fig. S2). However, a very limited amount of LAT

structure formation was noticed on the membrane after 5 min or 10 min of light irradiation, and no further LAT formation was found by prolonging the light exposure time (e.g., 30 and 45 min) (Fig. 3g). To confirm the formation of the LAT structures on the BDCA-LDNM, the production of ROS on the membrane after light irradiations was measured under a dark condition. As showcased in Fig. 3h, ROS was gradually generated from the membrane under dark after previous light treatments. The shortest light irradiation time (i.e., 5 min) resulted in the highest amount of ROS production, whereas the ROS production from the membrane after 30-min of light exposure was much lower (Fig. 3h). This phenomenon can be explained as the instant consumption of the LAT by thiyl radicals formed on the BDCA-LDNM during light irradiation. Afterward, the detoxification tailing property of the BDCA-LDNMs were evaluated by storing the detoxification system under dark right after daylight irradiations, and the detoxification results are plotted in Fig. 3i. There was no obvious difference in the detoxification amount of 1,3-D (i.e., around 3 mg/g) by BDCA-LDNM after 5 or 10 min of light treatments. However, after the light source was removed and stored for another 30 min, the detoxification amount of 1,3-D on the membrane with 10-min light exposure (detoxified 8.14 mg/g) was slightly higher than that of the 5-min one (detoxified 6.31 mg/g). On the other hand, to further prove that the detoxification tailing function was attributed to the LAT structure formation, the BDCA-LDNM was first charged by light for 10 min and then exposed to 1,3-D. Consequently, with the presence of the LAT structure on the membrane, 5.59 mg/g of 1,3-D was detoxified within 30 min under dark, whose efficiency achieved 58.29% to the one with sufficient light exposures. Consistent with the ROS production results, the long-term charging (e.g., 30 min) did not favor the LAT formation and storage, thus leading to less effective 1,3-D detoxification (i.e., 3.26 mg/g) under the a dark condition (Fig. 3i).

Therefore, the BDCA-LDNMs provide chemical protection against 1,3-D exposure not only under light irradiation but also under a situation with limited light sources, which is crucial for practical application, since most of the agricultural activities perform in the early morning.

3.4. Detoxification mechanism and practicability of LDNMs

The mechanism of the detoxification function of the BDCA-LDNM was investigated from both theoretical and experimental aspects. Firstly, DFT was employed to predict the ΔG of the proposed reaction between thiyl radical on BDCA and 1,3-D. As present in Fig. 4a, with light irradiation, the thiyl radicals on the BDCA-LDNM readily formed and are reactive to trans- or cis-1,3-D via thiol-ene click reactions. However, the two substitutions on both sides of the C=C bond in 1,3-D make it less reactive toward thiyl radicals to form a carbon-centered radical (denoted as BDCA-1,3-D•), whose ΔG values were calculated as 25.78 kJ/mol and 16.78 kJ/mol for trans- and cis-1,3-D, respectively, making this step not spontaneous at ambient condition. Nevertheless, the termination of the BDCA-1,3-D• via hydrogen abstraction to produce another thiyl radical is thermodynamically favorable, whose ΔG was calculated as –46.85 kJ/mol. Therefore, the favorability of the second step could drive the detoxification reaction to completion by showing the total ΔG values of the whole reaction between thiyl radical and 1,3-D as –21.07 kJ/mol and –30.07 kJ/mol for trans- and cis-1,3-D, respectively (Fig. 4a).

Furthermore, the dark condition and different samples were designed to obtain an insight into the necessity of photo-initiation and the presence of –SH groups for achieving the efficient detoxification function. Specifically, (i) dark condition was used to inhibit the photo-initiation of the BDCA-LDNM; (ii) 1,2,3,4-butanetetracarboxylic acid (BTCA), which contains equal mole of the reactive site to the BD (i.e., four carboxylic groups), was applied to replace the BD during LDNM modification, and the final material is denoted as BTCACA-LDNM; and (iii) ethanolamine was adopted to take over the role of CA on the LDNM, the final membrane is named as BDOH-LDNM. The chemical structures and characterizations of BTCACA-LDNM and BDOH-LDNM are available in the Supplementary Material (Fig. S3 and S4). Firstly, the detoxification of 1,3-D was performed on BDCA-LDNM under a dark condition. Without the photo-activation, no thiyl radicals can be formed on the membrane. Although the –SH groups could also react with 1,3-D via nucleophilic substitution reaction, the reaction rate was proved to be very slow, especially in a gas phase [29]. The achievement of BTCACA-LDNM is another way to avoid the photo-initiation process during the detoxification since BTCA lacks the photoactivity to trigger the formation of thiyl radicals even under light irradiation. On the contrary, the BDOH-LDNM maintains its photoactivity but lacks the –SH groups, causing no detoxification function of the membrane. As present in Fig. 4b, no decrease of the 1,3-D concentration can be found in any of the above situations, which indirectly proved the detoxification mechanism. The integrity of efficient photoactivity and massive –SH groups are indispensable to the ideal detoxifying LDNMs.

Moreover, the reaction between BDCA-LDNM and 1,3-D was modeled and investigated through ^{1}H NMR using the synthesized BDCA without the polymer base (see details in the Supplementary Material). As shown in Fig. 4c, new peaks showing at 3.96 ppm and 4.47 ppm belong to the protons in the 1,3-D fragments that have been linked to the –SH groups of BDCA. However, these peaks were not found if the sample was incubated with 1,3-D under a dark condition.

To illustrate the practicability of the BDCA-LDNMs for chemical protection. The detoxification of 1,3-D by BDCA-LDNMs were performed in an outdoor environment (i.e., in Davis, CA, USA; 38°32’18.9”N 121°44’59.5”W) under sunlight irradiation. The specific weather information of tested dates and times are summarized in Table 1. Although the light intensity and UV index varied significantly among the tested time points, the detoxification efficiency of the membrane was relatively constant. After 30 min of sunlight exposure, 50–60% of 30 μg/mL 1,3-D was detoxified, and the detoxification amount was calculated as 8.96–11.89 mg/g of the membrane (Fig. 4d), which are consistent with the results obtained in the laboratory under standard light sources (Fig. 3c). Given the mechanism of radical-mediated thiol-ene click reaction, the light-activated formation of thiyl radicals is crucial to the detoxification efficiency. The unique feature of BD moiety on the BDCA-LDNM, i.e., it can effectively activate the thiyl radical formation under UVA and daylight irradiations, and even under a dark condition, achieving the efficient detoxification function of BDCA-LDNM under diverse light irradiations. It makes the BDCA-LDNM promising for not only lab-based but also practical applications. Although we found a slight –SH concentration decrease (i.e., –SH retention = 79.07%) and photoactivity loss (i.e., ROS production retention = 72.25%) on the BDCA-LDNMs after 20-days of storage in a fridge at 4 °C under

dark, the detoxification efficiency of the BDCA-LDNMs retained 77.79% to that of the freshly made samples.

4. Conclusions

We demonstrated a facile approach of design and fabrication of the daylight-activated detoxifying materials (LDNMs) against 1,3-D, a model compound of ene-based toxicants, through the combination of nanofibrous membrane, photosensitizer, and biological thiols. The LDNMs can initiate the radical-mediated thiol-ene click reaction under daylight irradiation, thereby “switching on” the detoxification against 1,3-D. The detoxification efficiency is highly related to the photoactivity and the availability of sulfhydryl groups on the membrane. Given the formation of LAT structures on the LDNMs, the materials performed a detoxification tailing effect under dark conditions after a short-term light charging process. With the unique structure of LDNMs, they can efficiently detoxify 1,3-D vapor under light exposure or even under the dark condition. More importantly, the LDNMs showed robust chemical protection in an outdoor environment with the detoxification function efficiently activated by the sunlight. The successful development of LDNMs is promising for the design of innovative personal protective equipment with aggressive protection.

Supplementary Material

Refer to Web version on PubMed Central for supplementary material.

Acknowledgments

This work was financially supported by the California Department of Pesticide Regulation (18-C0012) and the National Institute of Environmental Health Sciences (NIEHS) (Grant No. 5P42ES004699). The authors are grateful to the Advanced Material Characterization and Testing Lab (AMCaT) at the University of California, Davis, for performing the SEM imaging. The author would like to thank the Department of Chemistry at the University of California, Davis, for providing the access to NMR testing.

References

[1]. Li Y, Miao R, Khanna M, Neonicotinoids and decline in bird biodiversity in the United States, Nat. Sustain. (2020).

[2]. Escher BI, Stapleton HM, Schymanski EL, Tracking complex mixtures of chemicals in our changing environment, Science 367 (2020) 388–392. [PubMed: 31974244]

[3]. Gruber K, Cleaning up our future health, Nature. 555 (2018) S20–S22.

[4]. McDonald BC, De Gouw JA, Gilman JB, Jathar SH, Akherati A, Cappa CD, Jimenez JL, Lee-Taylor J, Hayes PL, McKeen SA, Cui YY, Kim SW, Gentner DR, Isaacman-VanWertz G, Goldstein AH, Harley RA, Frost GJ, Roberts JM, Ryerson TB, Trainer M, Volatile chemical products emerging as largest petrochemical source of urban organic emissions, Science 359 (2018) 760–764. [PubMed: 29449485]

[5]. Larsen AE, Gaines SD, Deschênes O, Agricultural pesticide use and adverse birth outcomes in the San Joaquin Valley of California, Nat. Commun. 8 (2017) 1–8. [PubMed: 28232747]

[6]. Bradman A, Salvatore AL, Boeniger M, Castorina R, Snyder J, Barr DB, Jewell NP, Kavanagh-Baird G, Striley C, Eskenazi B, Community-based intervention to reduce pesticide exposure to farmworkers and potential take-home exposure to their families, J. Expo. Sci. Environ. Epidemiol. 19 (2009) 79–89. [PubMed: 18368011]

[7]. Ruzo LO, Physical, chemical and environmental properties of selected chemical alternatives for the pre-plant use of methyl bromide as soil fumigant, Pest Manag. Sci. 62 (2006) 99–113. [PubMed: 16308867]

[8]. The top 100 pesticides by pounds in total statewide pesticide use in 2017, California Department of Pesticide Regulation, available at: https://www.cdpr.ca.gov/docs/pur/pur17rep/top_100_ais_lbs_2017.htm (Accessed June 10, 2019).

[9]. Toxicological review of 1,3-Dichloropropene, Environmental Protection Agency, Available at: https://cfpub.epa.gov/ncea/iris/iris_documents/documents/toxreviews/0224tr.pdf (Accessed May 2000).

[10]. Si Y, Zhang Z, Wu W, Fu Q, Huang K, Nitin N, Ding B, Sun G, Daylight-driven rechargeable antibacterial and antiviral nanofibrous membranes for bioprotective applications, Sci. Adv. 4 (2018) 5931.

[11]. Ma Y, Zhang Z, Nitin N, Sun G, Integration of photo-induced biocidal and hydrophilic antifouling functions on nanofibrous membranes with demonstrated reduction of biofilm formation, J. Colloid Interface Sci. 578 (2020) 779–787. [PubMed: 32574911]

[12]. Tang P, Zhang M, Ji B, Yong T, Sun G, Hierarchical nucleophilic nanofibrous membranes for fast, durable, and bare-eye visible detoxification of carcinogenic alkylating toxicants, Adv. Funct. Mater. 29 (2019) 1905990.

[13]. Giannakoudakis DA, Barczak M, Florent M, Bandosz TJ, Analysis of interactions of mustard gas surrogate vapors with porous carbon textiles, Chem. Eng. J. 362 (2019) 758–766.

[14]. Florent M, Giannakoudakis DA, Wallace R, Bandosz TJ, Carbon textiles modified with copper-based reactive adsorbents as efficient media for detoxification of chemical warfare agents, ACS Appl. Mater. Interfaces. 9 (2017) 26965–26973. [PubMed: 28749134]

[15]. Kim S, Bin Ying W, Jung H, Ryu SG, Lee B, Lee KJ, Zirconium hydroxide-coated nanofiber mats for nerve agent decontamination, Chem. - An Asian J. 12 (2017) 698–705.

[16]. Yao A, Jiao X, Chen D, Li C, Bio-inspired polydopamine-mediated Zr-MOF fabrics for solar photothermal-driven instantaneous detoxification of chemical warfare agent simulants, ACS Appl. Mater. Interf. 12 (2020) 18437–18445.

[17]. Bromberg L, Su X, Martis V, Zhang Y, Hatton TA, Self-decontaminating fibrous materials reactive toward chemical threats, ACS Appl. Mater. Interfaces. 8 (2016) 17555–17564. [PubMed: 27309383]

[18]. Liang H, Yao A, Jiao X, Li C, Chen D, Fast and sustained degradation of chemical warfare agent simulants using flexible self-supported metal-organic framework filters, ACS Appl. Mater. Interfaces. 10 (2018) 20396–20403. [PubMed: 29806452]

[19]. Bromberg L, Creasy WR, McGarvey DJ, Wilusz E, Hatton TA, Nucleophilic polymers and gels in hydrolytic degradation of chemical warfare agents, ACS Appl. Mater. Interfaces. 7 (2015) 22001–22011. [PubMed: 26359671]

[20]. hui Wei X, Li C, Wang C, Lin S, Wu J, jie Guo M, Rapid and destructive adsorption of paraoxon-ethyl toxin via a self-detoxifying hybrid electrospun nanofibrous membrane, Chem. Eng. J. 351 (2018) 31–39.

[21]. Giannakoudakis DA, Hu Y, Florent M, Bandosz TJ, Smart textiles of MOF/g-C3N4 nanospheres for the rapid detection/detoxification of chemical warfare agents, Nanoscale Horizons. 2 (2017) 356–364. [PubMed: 32260666]

[22]. Del Giudice I, Coppolecchia R, Merone L, Porzio E, Carusone TM, Mandrich L, Worek F, Manco G, An efficient thermostable organophosphate hydrolase and its application in pesticide decontamination, Biotechnol. Bioeng. 113 (2016) 724–734. [PubMed: 26416557]

[23]. Singh A, Lee Y, Dressick WJ, Self-cleaning fabrics for decontamination of organophosphorous pesticides and related chemical agents, Adv. Mater. 16 (2004) 2112–2115.

[24]. Tang P, Leung HT, Gomez MT, Sun G, Sensitivity-tunable colorimetric detection of chloropicrin vapor on nylon-6 nanofibrous membrane based on a detoxification reaction with biological thiols, ACS Sensors. 3 (2018) 858–866. [PubMed: 29589433]

[25]. Tang P, Leung HT, Sun G, Colorimetric detection of carcinogenic alkylating fumigants on nylon-6 nanofibrous membrane. Part I: investigation of 4-(p-Nitrobenzyl)pyridine as a “new”

sensing agent with ultrahigh sensitivity, Anal. Chem. 90 (2018) 14593–14601. [PubMed: 30468706]

[26]. Tang P, Gomez MT, Leung HT, Sun G, Bio-inspired ultrasensitive colorimetric detection of methyl isothiocyanate on nylon-6 nanofibrous membrane: A comparison of biological thiol reactivities, J. Hazard. Mater. 362 (2019) 375–382. [PubMed: 30245405]

[27]. Tang P, Nguyen NT-H, Lo JG, Sun G, Colorimetric detection of carcinogenic alkylating fumigants on a nylon 6 nanofibrous membrane. Part II: self-catalysis of 2-diethylaminoethyl-modified sensor matrix for improvement of sensitivity, ACS Appl. Mater. Interf. 11 (2019) 13632–13641.

[28]. Wang Q, Gan J, Papiernik SK, Yates SR, Transformation and detoxification of halogenated fumigants by ammonium thiosulfate, Environ. Sci. Technol. 34 (2000) 3717–3721.

[29]. Bondarenko S, Zheng W, Yates SR, Gan J, Dehalogenation of halogenated fumigants by polysulfide salts, J. Agric. Food Chem. 54 (2006) 5503–5508. [PubMed: 16848538]

[30]. Zhong H, Zhu Z, You P, Lin J, Cheung CF, Lu VL, Yan F, Chan CY, Li G, Plasmonic and superhydrophobic self-decontaminating n95 respirators, ACS Nano. (2020).

[31]. Merenda A, Weber M, Bechelany M, Allioux FM, Hyde L, Kong L, Dumée LF, Fabrication of Pd-TiO2 nanotube photoactive junctions via atomic layer deposition for persistent pesticide pollutants degradation, Appl. Surf. Sci. (2019).

[32]. Yan L, Qin J, Kong L, Zhi H, Sun M, Shen G, Li L, Optimized synthesis of CuInS2/ZnS:Al-TiO2 nanocomposites for 1,3-dichloropropene photodegradation, RSC Adv. 6 (2016) 77777–77785.

[33]. Liu B, Deng X, Xie Z, Cheng Z, Yang P, Lin J, Thiol–ene click reaction as a facile and general approach for surface functionalization of colloidal nanocrystals, Adv. Mater. 29 (2017) 1–9.

[34]. Liu Y, Hou W, Sun H, Cui C, Zhang L, Jiang Y, Wu Y, Wang Y, Li J, Sumerlin BS, Liu Q, Tan W, Thiol-ene click chemistry: A biocompatible way for orthogonal bioconjugation of colloidal nanoparticles, Chem. Sci. 8 (2017) 6182–6187. [PubMed: 28989650]

[35]. Ellman GL, Tissue sulfhydryl groups, Arch. Biochem. Biophys. 82 (1959) 70–77. [PubMed: 13650640]

[36]. Zhang Z, Si Y, Sun G, Photoactivities of vitamin K derivatives and potential applications as daylight-activated antimicrobial agents, ACS Sustain. Chem. Eng. 7 (2019) 18493–18504.

[37]. Zhao C, Sun G, Catalytic actions of sodium salts in direct esterification of 3,3′4,4′-benzophenone tetracarboxylic acid with cellulose, Ind. Eng. Chem. Res. 54 (2015) 10553–10559.

[38]. Liang M, Wang F, Liu M, Yu J, Si Y, Ding B, N-Halamine functionalized electrospun poly(vinyl alcohol-co-ethylene) nanofibrous membranes with rechargeable antibacterial activity for bioprotective applications, Adv. Fiber Mater. 1 (2019) 126–136.

[39]. Arcot LR, Lundahl M, Rojas OJ, Laine J, Asymmetric cellulose nanocrystals : thiolation of reducing end groups via NHS – EDC coupling, Cellulose. 21 (2014) 4209–4218.

[40]. Shaterian HR, Ahmadian HR, Ghashang M, Doostmohammadi R, Yarahmadi H, Ferric hydrogensulfate as effective and recyclable catalyst for mild dithioacetalization of aldehydes and ketones, Phosphorus, Sulfur Silicon Relat. Elem. 183 (2008) 1099–1108.

[41]. Stache EE, Kottisch V, Fors BP, Photocontrolled radical polymerization from hydridic C-H bonds, J. Am. Chem. Soc. 142 (2020) 4581–4585. [PubMed: 32046481]

[42]. Roth M, Hennen D, Oesterreicher A, Mostegel FH, Kappaun S, Edler M, Griesser T, Exploring functionalized benzophenones as low-migration photoinitiators for vinyl carbonate/thiol formulations, Eur. Polym. J. 88 (2017) 403–411.

[43]. Bordoni AV, Lombardo MV, Wolosiuk A, Photochemical radical thiol-ene click-based methodologies for silica and transition metal oxides materials chemical modification: A mini-review, RSC Adv. 6 (2016) 77410–77426.

[44]. Dormán G, Nakamura H, Pulsipher A, Prestwich GD, The Life of Pi Star: Exploring the exciting and forbidden worlds of the benzophenone photophore, Chem. Rev. 116 (2016) 15284–15398. [PubMed: 27983805]

[45]. Marazzi M, Mai S, Roca-Sanjuán D, Delcey MG, Lindh R, González L, Monari A, Benzophenone ultrafast triplet population: revisiting the kinetic model by surface-hopping dynamics, J. Phys. Chem. Lett. 7 (2016) 622–626. [PubMed: 26821061]

[46]. Atkinson R, A structure-activity relationship for the estimation of rate constants for the gas-phase reactions of OH radicals with organic compounds, Int. J. Chem. Kinet. 19 (1987) 799–828.

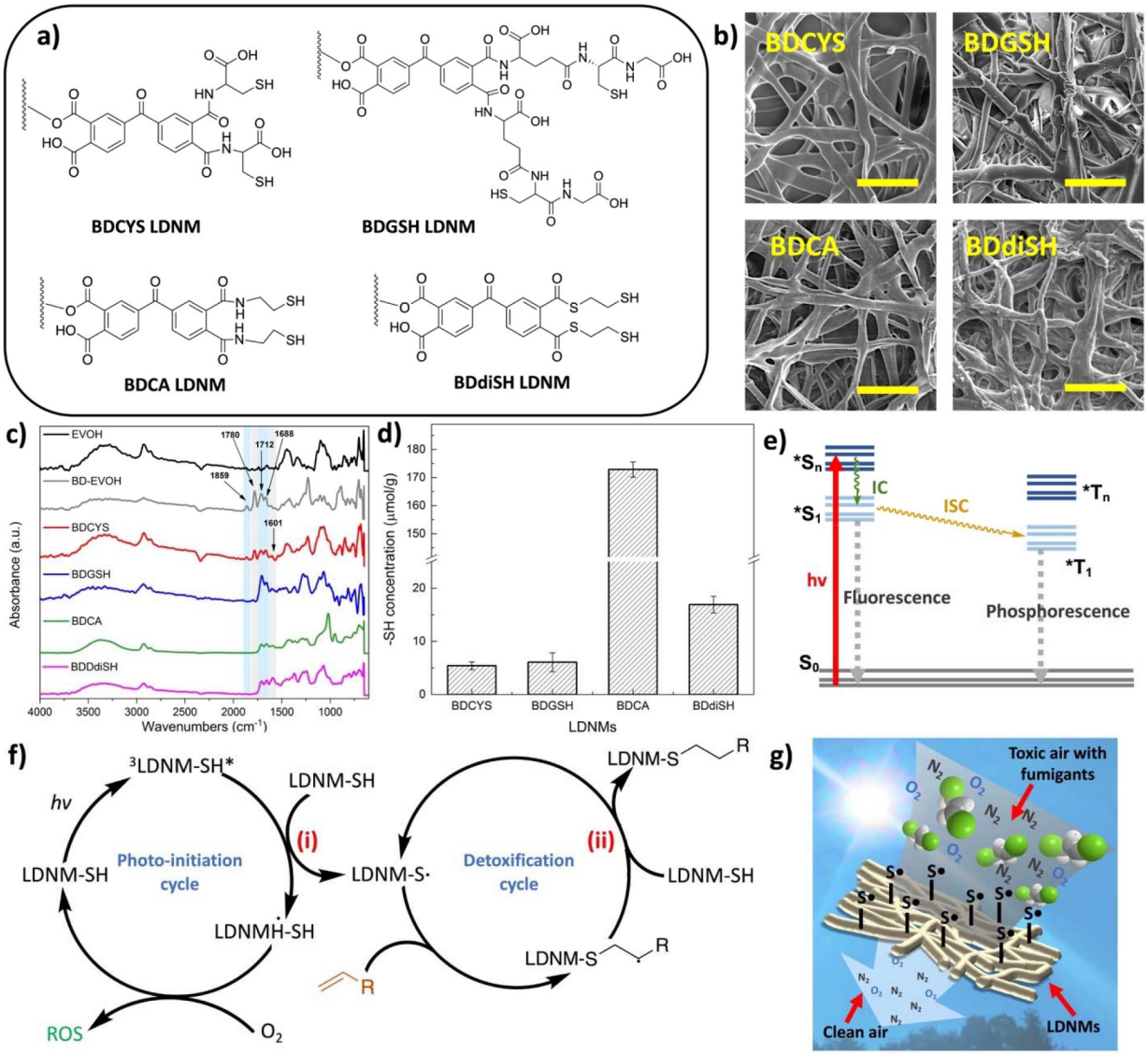

Fig. 1.

a) Chemical structures of BDCYS-LDNM, BDGSH-LDNM, BDCA-LDNM, and BDdiSH-LDNM. b) SEM images of different LDNMs. The yellow bar refers to 10 μm. Structural characterizations of LDNMs: c) ATR-FTIR spectra, and d) concentration of –SH groups on different LDNMs. e) Jablonski diagram representing the photoactivated function of LDNM by undergoing singlet excitation and ISC to triplet excited state. f) Proposed mechanism of the daylight-activated detoxification of ene-based toxicants by LDNMs via thiol-ene click reaction. g) Diagrammatic description of the detoxification function of LDNMs against 1,3-D under the light.

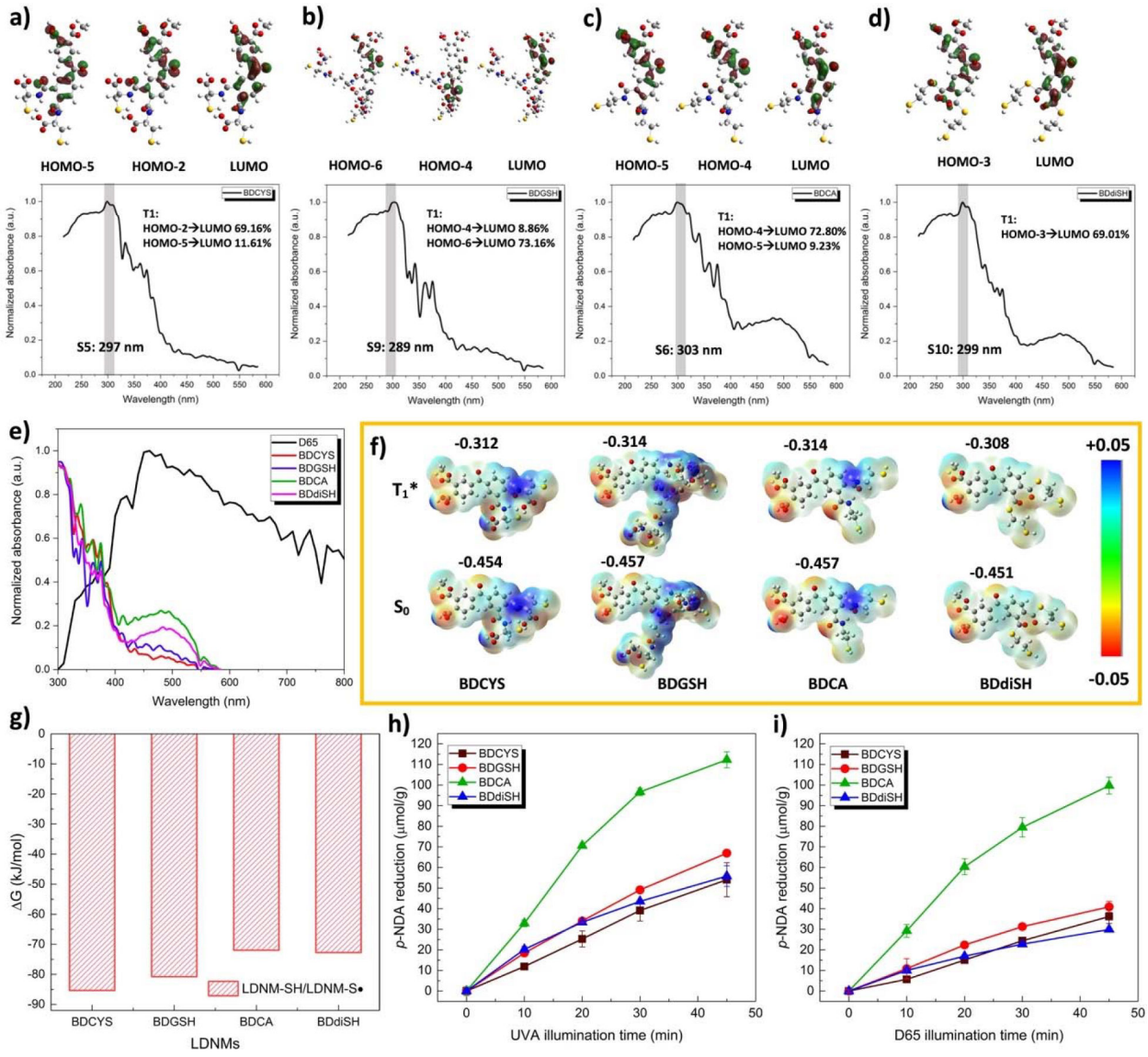

Fig. 2.

Diffuse reflectance UV-vis spectra of a) BDCYS-LDNM, b) BDGSH-LDNM, c) BDCA-LDNM, and d) BDdiSH-LDNM with theoretically assigned contributions of T_1 orbitals. The acronyms of HOMO and LUMO are the highest occupied molecular orbital and the lowest unoccupied molecular orbital, respectively. Atom labels: grey = carbon, white = hydrogen, red = oxygen, blue = nitrogen, yellow = sulfur. e) Normalized UV-vis spectra of LDNMs accompanied with the D65 standard light source. f) Electrostatic potential map of different LDNMs at ground states and triplet excited states. The values labeled in the figure stand for the charges on the oxygen atoms in carbonyl groups. g) Theoretically calculated Gibbs free energy changes of thiyl radical formation on different LDNMs induced by the triplet state of corresponding LDNMs. Measurements of ROS production on different LDNMs under h) UVA and i) daylight (D65) irradiation.

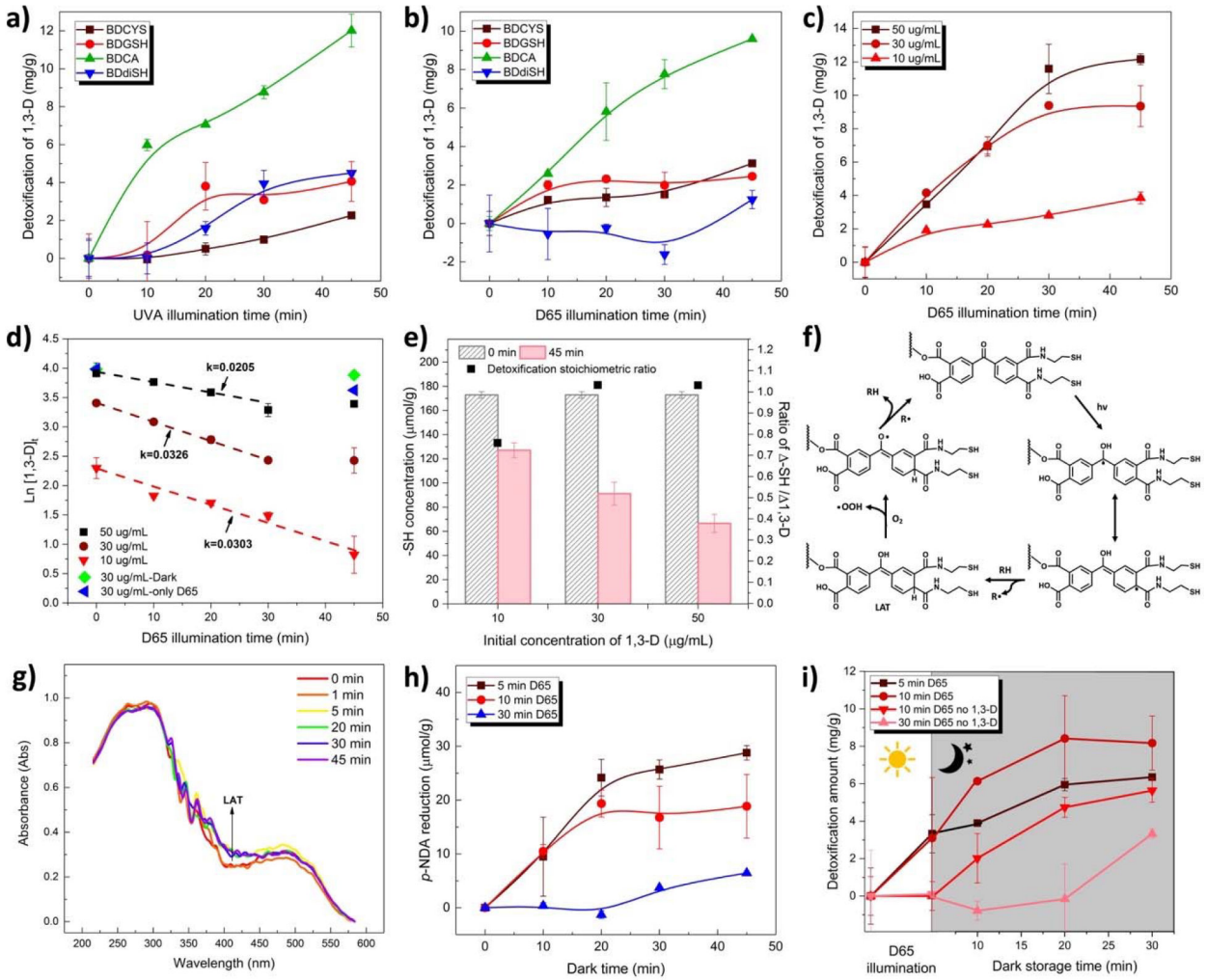

Fig. 3.

Detoxification performance against 1,3-D (30 μg/mL) by different LDNMs under a) UVA and b) daylight (D65) irradiation. c) Detoxification amount on BDCA-LDNMs against different initial concentrations of 1,3-D. d) Pseudo-first order kinetics of 1,3-D detoxification by BDCA-LDNM under daylight irradiation. e) Sulfhydryl concentration on the BDCA-LDNMs after 1,3-D detoxification, and the stoichiometric ratio between –SH consumption and 1,3-D detoxification (Δ–SH/Δ1,3-D). f) Schematic illustration of LAT structure formation and quenching cycle on BDCA-LDNM. g) Diffuse reflection UV-vis spectra of BDCA LDNM under increasing daylight irradiation time. h) ROS production on BDCA-LDNM under a dark condition after different daylight irradiation time. i) Detoxification tailing effect of BDCA-LDNM against 1,3-D (30 μg/mL) under a dark condition after different durations of daylight irradiation.

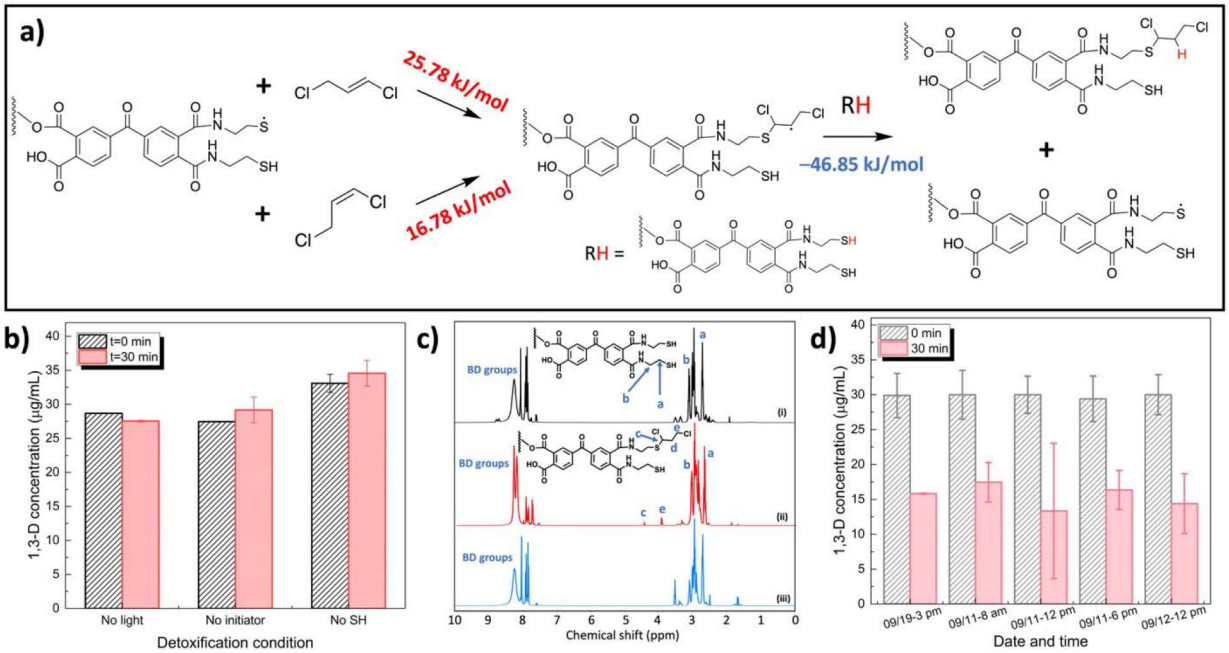

Fig. 4.

a) Gaussian calculated Gibbs free energy changes of the detoxification reaction between 1,3-D and BDCA-LDNM. b) Detoxification results of BDCA-LDNM under specific conditions. c) ^{1}H NMR spectra BDCA (i) before and after detoxification against 1,3-D with (ii) daylight irradiation and (iii) dark storage for 60 min. d) Outdoor detoxification results of BDCA-LDNMs against 1,3-D on/at different dates and time points.

Table 1.

Conditions of the outdoor detoxification.

Date	Time	Light intensity (kLux)[a]	Temperature (°C)[b]	Relative humidity[b]	UV index[b]
09/10/2020	3:00–3:30 pm	10.4	27	31%	5
09/11/2020	8:00–8:30 am	6.9	13	83%	1
09/11/2020	12:00–12:30 pm	29.2	24	46%	6
09/11/2020	6:00–6:30 pm	5.7	29	30%	1
09/12/2020	12:00–12:30 pm	36.8	26	41%	6

[a] The values were measured by a light meter (EXTECH, Model # LT300).

[b] The values were read from a weather application installed on the iPhone.